Progress In Electromagnetics Research, PIER 38, 223–252, 2002

A SPECTRAL-DOMAIN SOLUTION FOR THE SCATTERING PROBLEM OF A CIRCULAR CYLINDER BURIED IN A DIELECTRIC HALF-SPACE

F. Ciambra

Alemia Marconi Systems
Via Tiburtina Km 12,400, I-00131 Rome, Italy

F. Frezza and L. Pajewski

Dip. di Ingegneria Elettronica, Università La Sapienza
Via Eudossiana 18, I-00184 Rome, Italy

G. Schettini

Dip. di Applicata Elettronica, Università Roma Tre
Via della Vasca Navale 84, I-00146 Rome, Italy

Abstract—A spectral-domain solution is employed to completely characterize the two-dimensional electromagnetic plane-wave scattering problem by a perfectly conducting circular cylinder buried in a dielectric half-space. Use is made of the plane-wave spectrum to consider the diffraction, reflection and transmission of cylindrical waves. Suitable adaptive integration techniques are employed to numerically solve the spectral integrals. The method is valid for any value of the cylinder radius, and of the distance between the cylinder and the interface. Numerical results are presented for both near- and far-field cases and for both TM and TE polarizations, and a comparison with other results in the literature is discussed.

1. INTRODUCTION

The electromagnetic scattering problem of buried obstacles has been discussed by many authors in the past, both from a theoretical [1, 2] and a numerical [3, 4] point of view, due to its application to remote sensing of the earth's subsurface or to communication through the earth. Many different techniques have been used. In particular, Howard [1] employed the mode-matching method to solve a two-dimensional integral equation for the scattered field. Ogunade [5] extended an early work [6] allowing one to obtain more easily numerical results. Mahmoud *et al.* [7] faced the problem using a multipole expansion of the scattered field. Butler *et al.* [8] solved an integral equation for the induced current, discussing various forms of the kernel suitable for an efficient numerical evaluation. Hongo *et al.* [9] treated the plane-wave scattering by a two-dimensional cylindrical obstacle in a dielectric half-space employing the Kobayashi potential concept [10]. The asymptotic solutions presented, using the saddle-point method, are valid for the obstacle size and the distance between the obstacle and the interface much greater than the wavelength. A corrected version of paper [9] has been reported in [11].

In this paper we consider the two-dimensional plane-wave scattering problem by a perfectly conducting circular cylinder buried in a dielectric half-space. As is well known, the field scattered by the object can be decomposed in cylindrical waves, i.e., the product of a Hankel function times an exponential angular factor. The concept of plane-wave spectrum of a cylindrical wave [12] has been employed. The reflection properties of such cylindrical waves in the presence of plane interfaces have been discussed in [13], by introducing suitable reflected cylindrical functions. However, in that case, the cylindrical obstacle was in the same half-space of the incident wave. In this work, instead, the main interest is in the transmission of the cylindrical waves outside the dielectric half-space in which the obstacle is buried. To this aim, suitable transmitted cylindrical

functions are here introduced and the relevant spectral integrals are considered. In the case of a general dielectric medium characterized by its reflection and transmission coefficients, the spectral integrals have been numerically solved employing suitable adaptive integration techniques of Gaussian type, together with convergence acceleration algorithms [14, 15]. The proposed method may deal with both TM and TE polarization cases and yields results in both the near- and the far-field zones. The first case is important for applications to Surface Penetrating Radar (SPR) [16], which usually employ purely numerical FDTD techniques [17]. Moreover, our method may be applied for any value of the obstacle size and of the distance between the obstacle and the surface.

In Sect. 2 the analytical characteristics of the approach are described. In Sect. 3 the relevant numerical solution is presented. Finally, in Sect. 4 numerical results are presented for both TM and TE polarizations both in the near and in the far region. A parametric analysis has been performed showing the influence of the geometrical dimensions and of the incidence angle. Moreover, a comparison is made with the results presented in [11].

2. THEORETICAL ANALYSIS

The geometry of the problem is shown in Fig. 1. A perfectly conducting circular cylinder with radius a is buried in a linear, isotropic, homogeneous dielectric medium (medium 1). We consider a rectangular coordinate frame (x, y, z) centered on the cylinder axis, which is coincident with the y axis and placed at a distance h from a plane interface with a different linear, isotropic, homogeneous, dielectric medium (medium 0). A monochromatic plane wave, with wavelength λ and wavevector $\mathbf{k}_\mathrm{i}$ lying in the xz plane, comes from medium 0 and obliquely impinges on the interface with medium 1; φ is the angle between $\mathbf{k}_\mathrm{i}$ and the x axis. The structure is assumed to be infinite along the y direction, so that the analyzed problem is two-dimensional.

As is well known, the incident polarization may be decomposed into the two fundamental cases of TM or E (electric field parallel to the cylinder axis) and TE or H (magnetic field parallel to the cylinder axis) polarizations. The time dependence of the field is assumed to be $e^{-i\omega t}$, where ω is the angular frequency, and throughout the paper will be omitted.

The following dimensionless notation is used, where the spatial variables are normalized to the vacuum wavenumber $k = 2\pi/\lambda$: $\xi = kx$, $\zeta = kz$, $\chi = kh$, and $\alpha = ka$. A polar coordinate system

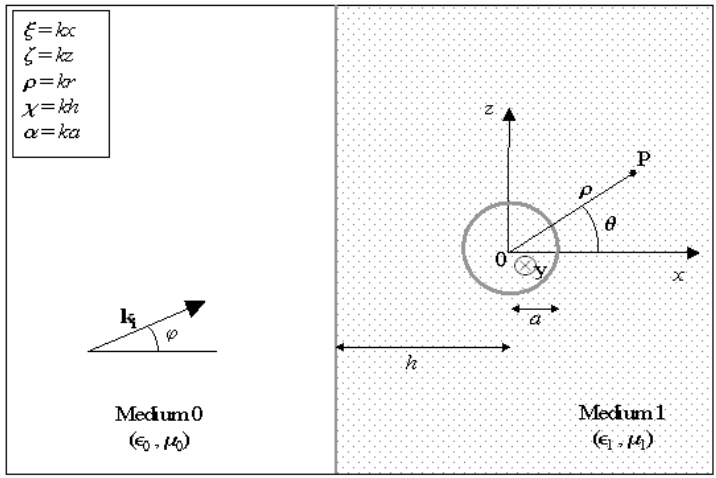

Figure 1. Geometry of the scattering problem.

(ρ, ϑ), with $\rho = kr$, centered on the cylinder axis, is also introduced.

The incident wavevector $\mathbf{k}_\mathrm{i}$ is related to the angle φ as follows: $k^\mathrm{i}_\perp = k\cos\varphi$ and $k^\mathrm{i}_{//} = k\sin\varphi$. $k^\mathrm{i}_\perp$ and $k^\mathrm{i}_{//}$ are the orthogonal and parallel components of the wavevector with respect to the interface, respectively. The presence of the interface is described by the complex angle-dependent reflection and transmission coefficients $\Gamma(n_{//})$ and $T(n_{//})$, where $\mathbf{n} = \mathbf{k}/k$ is the unit vector parallel to the generic wavevector $\mathbf{k}$.

The solution is carried out in terms of $V(\xi, \zeta)$, which represents the electromagnetic field component parallel to the y axis: $V = E_\mathrm{y}$ for TM polarization and $V = H_\mathrm{y}$ for TE polarization. Once $V(\xi, \zeta)$ is known, it is obviously possible to derive all the remaining components of the electromagnetic field using Maxwell's equations. In order to rigorously obtain a closed-form solution for $V(\xi, \zeta)$, the total field is expressed as the superposition of the following six terms, produced by the interaction between the incident field and the interface-cylinder system (see Fig. 2):

- $V_\mathrm{i}(\xi, \zeta)$, field of the incident plane wave;
- $V_\mathrm{r}(\xi, \zeta)$, field of the reflected plane wave, due to the reflection of V_i by the plane interface;
- $V_\mathrm{t}(\xi, \zeta)$, field of the plane wave transmitted in medium 1 by the plane interface;

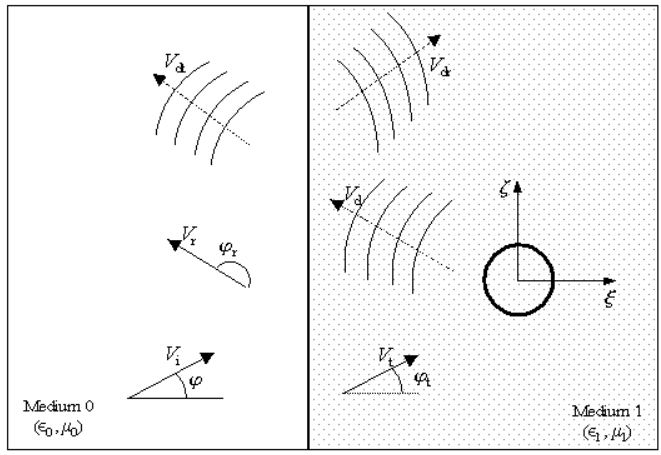

Figure 2. Decomposition of the total field in six terms.

- $V_{\mathrm{d}}(\xi, \zeta)$, field diffracted by the conducting cylinder in medium 1;
- $V_{\mathrm{dr}}(\xi, \zeta)$, diffracted-reflected field, due to the reflection of V_{d} by the plane interface;
- $V_{\mathrm{dt}}(\xi, \zeta)$, diffracted-transmitted field, due to the transmission of V_{d} by the plane interface.

A similar decomposition has been adopted in [13]. In order to take into account transmission effects, here we introduce two more terms, V_{t} and V_{dt}.

Because of the cylindrical geometry of the problem, it is useful to express all the above mentioned fields in terms of functions that show cylindrical symmetry, centered on the cylinder axis. The solution procedure may be summarized as follows. The known fields V_{i}, V_{r}, and V_{t} may be expressed by using the customary expansion of a plane wave in terms of Bessel functions [18]. The unknown field V_{d} may be expressed as a series of two-dimensional cylindrical waves. As far as the expressions of the unknown fields V_{dr} and V_{dt} are concerned, expansions in generalized reflected and transmitted cylindrical waves may be used, following an approach similar to that outlined in [13]. The use of the analytical plane-wave spectrum of the cylindrical waves allows us to exploit the plane-wave reflection and transmission coefficients of the interface. Imposing the boundary conditions on the surface of the circular conducting cylinder, we obtain a linear system for the unknown expansion coefficients.

Assuming without loss of generality medium 0 as a vacuum, the expressions of the incident and of the reflected plane waves $V_{\rm i}(\xi,\zeta)$ and $V_{\rm r}(\xi,\zeta)$ are:

$$V_{\rm i}(\xi,\zeta) = V_0 e^{i(n^{\rm i}_{\perp}\xi + n^{i}_{//}\zeta)} = V_0 \sum_{m=-\infty}^{+\infty} i^m J_m(\rho) e^{im\vartheta} e^{-im\varphi} \qquad (1)$$

and

$$\begin{aligned} V_{\rm r}(\xi,\zeta) &= V_0 \Gamma(n^{i}_{//}) e^{i[n^{i}_{\perp}(-\xi-2\chi)+n^{i}_{//}\zeta]} \\ &= V_0 \Gamma(n^{i}_{//}) e^{-in^{i}_{\perp}2\chi} \sum_{m=-\infty}^{+\infty} i^m J_m(\rho) e^{im\vartheta} e^{-im\varphi_{\rm r}}, \end{aligned} \qquad (2)$$

where V_0 is a complex amplitude, $n^{\rm i}_{\perp} = \cos\varphi$ and $n^{\rm i}_{//} = \sin\varphi$ are the orthogonal and parallel normalized components of the incident wavevector, respectively, $\Gamma(n^{\rm i}_{//})$ is the reflection coefficient from medium 0 to medium 1, and $\varphi_{\rm r} = \pi - \varphi$.

For the transmitted plane-wave field $V_{\rm t}(\xi,\zeta)$ we have:

$$\begin{aligned} V_{\rm t}(\xi,\zeta) &= V_0 T(n^{\rm i}_{//}) e^{in_1(n^{\rm t}_{\perp}\xi + n^{\rm t}_{//}\zeta)} \\ &= V_0 T(n^{\rm i}_{//}) \sum_{m=-\infty}^{+\infty} i^m J_m(\rho) e^{im\vartheta} e^{-im\varphi_{\rm t}}, \end{aligned} \qquad (3)$$

where $T(n^{\rm i}_{//})$ is the transmission coefficient from medium 0 to medium 1, n_1 is the refractive index of medium 1, $n^{\rm t}_{\perp}$ and $n^{\rm t}_{//}$ are the orthogonal and parallel normalized components of the transmitted plane-wave wavevector, respectively, and $\varphi_{\rm t} = \arcsin(\frac{1}{n_1}\sin\varphi)$. In Eqs. (1), (2), and (3) the known expansion of a plane wave in terms of first-kind Bessel functions $J_m(\rho)$ has been used.

As is known, the diffracted field $V_{\rm d}(\xi,\zeta)$ may be expressed as the superposition of cylindrical functions $CW_l(\xi,\zeta) = H^{(1)}_l(\rho)e^{il\theta}$, where $H^{(1)}_l$ is a first-kind Hankel function of integer order and conversion between polar and rectangular coordinates is assumed. Therefore for $V_{\rm d}(\xi,\zeta)$ we have:

$$V_{\rm d}(\xi,\zeta) = V_0 \sum_{l=-\infty}^{+\infty} i^l e^{-il\varphi_t} c_l CW_l(n_1\xi, n_1\zeta), \qquad (4)$$

where c_l are the unknown expansion coefficients and the term $i^l e^{-il\varphi_t}$ has been explicitated in order to simplify the imposition of boundary

conditions; the refractive index n_1 is present in the arguments of the CW_l functions since these functions have to be used in medium 1.

The diffracted-reflected field $V_{\mathrm{dr}}(\xi,\zeta)$ may be expressed as the superposition of all the field configurations produced in the reflection by the plane interface of each cylindrical wave CW_l in Eq. (4). With an approach analogous to that in [13], we obtain:

$$V_{\mathrm{dr}}(\xi,\zeta) = V_0 \sum_{l=-\infty}^{+\infty} i^l e^{-il\varphi_t} c_l RW_l[n_1(-\xi-2\chi), n_1\zeta], \tag{5}$$

where $RW_l(\xi,\zeta)$ are the reflected cylindrical wave functions, which have the following expression:

$$RW_l(\xi,\zeta) = \frac{1}{2\pi} \int_{-\infty}^{+\infty} \Gamma(n_{//}) F_l(\xi, n_{//}) e^{in_{//}\zeta} dn_{//}, \tag{6}$$

and

$$F_l(\xi, n_{//}) = \int_{-\infty}^{+\infty} CW_l(\xi,\zeta) e^{-in_{//}\zeta} d\zeta \tag{7}$$

is the plane-wave spectrum of the cylindrical functions CW_l. The explicit expression of F_l is [13]:

$$F_l(\xi, n_{//}) = \frac{2}{\sqrt{1-n_{//}^2}} e^{i\left[\xi\sqrt{1-n_{//}^2} - l\arccos(n_{//})\right]}, \tag{8}$$

where the function arccos is meant to be defined over the whole real axis. Note that this expression is valid when $\xi > 0$; if $\xi < 0$, it is useful to keep in mind the parity property of the function $F_l(\xi, n_{//})$ [12], which in the present coordinate system turns out to be $F_l(\xi, n_{//}) = F_{-l}(|\xi|, n_{//})$.

Starting from Eq. (5), making use of Eq. (6), of the expansion of a plane wave in terms of first-kind Bessel functions, and of Eq. (8) with its parity property, after some manipulations [13] we obtain:

$$V_{\mathrm{dr}}(\xi,\zeta) = V_0 \sum_{l=-\infty}^{+\infty} i^l e^{-il\varphi_t} c_l \sum_{m=-\infty}^{+\infty} J_m(n_1\rho) e^{im\vartheta} RW_{l-m}(-2n_1\chi, 0). \tag{9}$$

The contribution due to the propagation of the generic spectral component of the V_{dr} field up to the interface from medium 1 toward medium 0 (i.e. in $\xi = -\chi$) is:

$$F_l(-n_1\chi, n_{//}^1) = F_l(0, n_{//}^1) e^{in_1 n_\perp^1(-\chi)}. \tag{10}$$

Here, $n_{\perp}^{1}$ and $n_{//}^{1}$ are the orthogonal and parallel components, respectively, of the unit wavevector associated with the generic component of the spectrum F_l in medium 1.

The diffracted-transmitted field $V_{\rm dt}(\xi,\zeta)$ may be expressed as the superposition of all the field configurations produced in the transmission by the plane interface of each cylindrical wave CW_l of Eq. (4) from medium 1 to medium 0. In the generic plane $\xi = \xi_0 < -\chi$, the contribution (10) to the diffracted-transmitted field becomes:

$$T(n_{//}^{1})F_l(-n_1\chi, n_{//})e^{in_{\perp}^{0}(\xi_0+\chi)}. \tag{11}$$

In Eq. (11) $n_{\perp}^{0}$ is the orthogonal component of the unit wavevector associated with the generic spectral component transmitted from medium 1 to medium 0, and $T(n_{//}^{1})$ is the relevant transmission coefficient. Calling $n_{//}^{0}$ the parallel component of the unit vector, and taking into account Snell's law, we have:

$$\begin{cases} n_{\perp}^{0} = \sqrt{1 - n_1^2[1-(n_{\perp}^{1})^2]} \\ n_{//}^{0} = n_1 n_{//}^{1}. \end{cases} \tag{12}$$

We introduce now the transmitted cylindrical waves $TW_l(\xi,\zeta)$

$$TW_l(\xi,\zeta) = \frac{1}{2\pi}\int_{-\infty}^{+\infty} T(n_{//}^{1})F_l(-n_1\chi, n_{//}^{1})e^{-in_{\perp}^{0}(\xi+\chi)}e^{in_{//}^{0}\zeta}dn_{//}^{1} \tag{13}$$

(in the left-hand side, and in the following, the dependence from χ and n_1 has been suppressed for brevity), so that the whole diffracted-transmitted field $V_{\rm dt}(\xi,\zeta)$ can be written as:

$$V_{\rm dt}(\xi,\zeta) = V_0\sum_{l=-\infty}^{+\infty} i^l e^{-il\varphi_t}c_l TW_l(\xi,\zeta), \tag{14}$$

which is similar to expressions (4) and (5) for $V_{\rm d}$ and $V_{\rm dr}$, respectively.

Once the expressions of all fields have been given, we have to impose the boundary conditions on the surface of the circular conducting cylinder buried in medium 1, namely $[V_{\rm t}+V_{\rm d}+V_{\rm dr}]_{\rho=\alpha} = 0$ for TM polarization, and $[V_{\rm t}+V_{\rm d}+V_{\rm dr}]'_{\rho=\alpha} = 0$ for TE polarization, where the prime denotes derivation with respect to variable ρ. By using the expressions of the fields given in Eqs. (3), (4), and (9), after some algebra we obtain the following linear system for the unknown coefficients c_l:

$$\sum_{l=-\infty}^{+\infty} A_{ml}c_l = b_m \qquad\qquad (m = 0; \pm 1; \pm 2\ldots), \tag{15}$$

where

$$A_{ml} = e^{-il\varphi_t}\left[i^{l-m}G_m(n_1\alpha)RW_{l-m}(-2n_1\chi,0)+\delta_{ml}\right], \quad (16)$$

$$b_m = -T(n_{//}^{\mathrm{i}})G_m(n_1\alpha)e^{-im\varphi_{\mathrm{t}}}, \quad (17)$$

and δ_{ml} is the Kronecker symbol. The function G_m is defined as:

$$G_m(u) = \begin{cases} \dfrac{J_m(u)}{H_m^{(1)}(u)} & \text{for TM polarization} \\ \dfrac{J'_m(u)}{H'^{(1)}_m(u)} & \text{for TE polarization.} \end{cases} \quad (18)$$

Once the linear system (15) has been solved, and the coefficients c_l have been calculated, it is possible to evaluate the total electric (magnetic) field for TM (TE) polarization, in any point (ξ,ζ) outside the conducting cylinder, both in medium 0 and in medium 1. In fact, the total field in medium 0 is $V_0(\xi,\zeta) = V_{\mathrm{i}}(\xi,\zeta) + V_{\mathrm{r}}(\xi,\zeta) + V_{\mathrm{dt}}(\xi,\zeta)$, while in medium 1 it is $V_1(\xi,\zeta) = V_{\mathrm{t}}(\xi,\zeta) + V_{\mathrm{d}}(\xi,\zeta) + V_{\mathrm{dr}}(\xi,\zeta)$.

By using Maxwell's equations, it is now possible to derive the total electromagnetic field both in medium 0 and in medium 1. For example, for TM polarization we obtain: $\mathbf{E}(\xi,\zeta) = V(\xi,\zeta)\boldsymbol{y}_0$ and $\mathbf{H}(\xi,\zeta) = -\frac{i}{\omega\mu}\nabla\times\mathbf{E} = iY\frac{\partial V(\xi,\zeta)}{\partial\zeta}\boldsymbol{\xi}_0 - iY\frac{\partial V(\xi,\zeta)}{\partial\xi}\boldsymbol{\zeta}_0$, where Y is the characteristic admittance. It is apparent that to evaluate the total electromagnetic field, it is necessary to use the partial derivatives of $V(\xi,\zeta)$ with respect to variables ξ and ζ. Since the total field in medium 1 is expressed in terms of the cylindrical wave functions $CW_l(\xi,\zeta)$, and of the cylindrical reflected wave functions $RW_l(\xi,\zeta)$, it is necessary to calculate the expressions of the partial derivatives of such functions. Such derivatives are given in [13]. To obtain the total field in medium 0, on the other hand, the expressions of the partial derivatives of the cylindrical transmitted wave functions $TW_l(\xi,\zeta)$ are necessary; following an approach similar to that outlined in [13], we have (see appendix A):

$$\frac{\partial TW_l(\xi,\zeta)}{\partial\xi} = -\frac{i}{2\pi}\int_{-\infty}^{+\infty} n_\perp^0 T(n_{//}^1)F_l(-n_1\chi,n_{//})e^{-in_\perp^0(\xi+\chi)}e^{in_{//}^0\zeta}dn_{//}^1, \quad (19)$$

and

$$\frac{\partial TW_l(\xi,\zeta)}{\partial\zeta} = \frac{in_1}{2}[TW_{l+1}(\xi,\zeta) + TW_{l-1}(\xi,\zeta)]. \quad (20)$$

3. NUMERICAL SOLUTION

When dealing with numerical procedures, it is obviously necessary to truncate the series of Eq. (15) to a finite number of elements:

$$\sum_{l=-M}^{+M} A_{ml} c_l = b_m \qquad (m = 0, \pm 1, ..., \pm \mathrm{M}). \tag{21}$$

As suggested in [19] and [20], the choice $M \cong 3\alpha$ is an efficient truncation criterion, showing a very good compromise between accuracy and computational heaviness. In Sect. 4 the validity of such criterion is verified for two different cases.

The evaluation of the generalized cylindrical reflected and transmitted wave functions $RW_l(\xi, \zeta)$ (see Eq.(6)) and

$$TW_l(\xi, \zeta) = \frac{1}{2\pi} \int_{-\infty}^{+\infty} T(n_{//}) F_l(-n_1 \chi, n_{//}) e^{-i\sqrt{1-n_1^2 n_{//}^2}(\xi+\chi)} e^{i n_1 n_{//} \zeta} dn_{//}, \tag{22}$$

has to be carried out numerically (Eq. (22) derives from Eqs. (12) and (13), where for simplicity we put $n_{//}^1 = n_{//}$). In fact, in all practical cases, the expressions of the reflection and transmission coefficients Γ and T do not allow an analytical evaluation of the integrals in Eqs. (6) and (22).

In order to develop an efficient integration algorithm, one has to take into account the infinite extension of the integration domain, since the solution cannot neglect the evanescent components of the spectrum (near-field solution). Moreover, the spectrum of the cylindrical wave functions shows a highly oscillating behavior [21] as the expansion order l increases. A suitable algorithm for the integration of the functions $RW_l(\xi, \zeta)$ has been developed in [14] and [15]. In the following, the algorithm will be generalized to integrate also the functions $TW_l(\xi, \zeta)$.

To well understand the behavior of the integrand of Eq. (22) as $n_{//}$ varies over the whole real axis, it may be useful to consider the explicit expression of the spectrum of the cylindrical functions for $\xi < 0$:

$$F_l(\xi, n_{//}) = \begin{cases} \dfrac{2e^{i|\xi|\sqrt{1-n_{//}^2}}}{\sqrt{1-n_{//}^2}} (\sqrt{n_{//}^2 - 1} + n_{//})^{-l} & \text{for} \quad |n_{//}| > 1 \\ \dfrac{2e^{i|\xi|\sqrt{1-n_{//}^2}}}{\sqrt{1-n_{//}^2}} e^{il \arccos(n_{//})} & \text{for} \quad |n_{//}| < 1. \end{cases} \tag{23}$$

Eq. (23) suggests a first decomposition of the integration domain, so that Eq. (22) can be rewritten as follows:

$$\begin{aligned} TW_l(\xi,\zeta) &= \frac{1}{2\pi}\int\limits_{|n_{//}|>1} T(n_{//})F_l(-n_1\chi,n_{//}) \\ &\quad e^{-i\sqrt{1-n_1^2n_{//}^2}(\xi+\chi)}e^{in_1n_{//}\zeta}dn_{//} \\ &\quad +\frac{1}{2\pi}\int\limits_{|n_{//}|<1} T(n_{//})F_l(-n_1\chi,n_{//}) \\ &\quad e^{-i\sqrt{1-n_1^2n_{//}^2}(\xi+\chi)}e^{in_1n_{//}\zeta}dn_{//}. \end{aligned} \tag{24}$$

The first integral in Eq. (24) represents the contribution to $TW_l(\xi,\zeta)$ of the evanescent spectral plane waves of the spatial Fourier spectrum; the second integral in Eq. (24) is the contribution of the homogeneous spectral plane waves. These two contributions will be separately evaluated. Defining:

$$\begin{aligned} I_l^{(\mathrm{ext})}(\xi,\zeta) &= \int\limits_{|n_{//}|>1} T(n_{//})\frac{e^{-n_1\chi\sqrt{n_{//}^2-1}}}{\sqrt{n_{//}^2-1}}(\sqrt{n_{//}^2-1}+n_{//})^{-l} \\ &\quad e^{\sqrt{n_1^2n_{//}^2-1}(\xi+\chi)}e^{in_1n_{//}\zeta}dn_{//} \end{aligned} \tag{25}$$

and

$$\begin{aligned} I_l^{(\mathrm{int})}(\xi,\zeta) &= \int\limits_{|n_{//}|<1} T(n_{//})\frac{e^{i|n_1\chi|\sqrt{1-n_{//}^2}}}{\sqrt{1-n_{//}^2}}e^{il\arccos(n_{//})} \\ &\quad e^{-i\sqrt{1-n_1^2n_{//}^2}(\xi+\chi)}e^{in_1n_{//}\zeta}dn_{//}, \end{aligned} \tag{26}$$

after some manipulations, the expression of $TW_l(\xi,\zeta)$ becomes:

$$TW_l(\xi,\zeta) = \frac{1}{\pi}\left[I_l^{(int)}(\xi,\zeta) - iI_l^{(ext)}(\xi,\zeta)\right]. \tag{27}$$

3.1. Integration of the Evanescent Spectrum

The integrand of Eq. (25) presents a singularity in $|n_{//}| = 1$, which can be removed with the position $n_{//} = \sqrt{t^2+1}$; moreover, assuming the

parity of the transmission coefficient, after some algebra we obtain:

$$I_l^{(\mathrm{ext})}(\xi,\zeta) = Q_l(\xi,\zeta) + (-1)^l Q_{-l}(\xi,-\zeta), \tag{28}$$

where

$$Q_l(\xi,\zeta) = \int_{t=0}^{+\infty} T[\cos(t)] \frac{(\sqrt{t^2+1}+t)^{-l}}{\sqrt{t^2+1}} e^{-n_1\chi t} e^{\sqrt{n_1^2t^2+n_1^2-1}(\xi+\chi)} e^{in_1\zeta\sqrt{t^2+1}} dt. \tag{29}$$

To solve the integral (29) we followed the approach proposed in [14], i.e. we adopted a generalized Gaussian integration method, consisting in a decomposition of the integration interval in subintervals of suitable length on which a fixed low-order Gaussian rule (for example Gauss-Legendre rule) gives good accuracy.

3.2. Integration of the Homogeneous Spectrum

Let us now consider the integral (26). Studying how the sign of the square-root arguments in Eq. (26) vary as a function of $n_{//}$, and keeping in mind that $|n_{//}| < 1$, $n_1 > 1$ and $\chi > 0$, it is possible to decompose Eq. (26) into two terms, as follows:

$$I_l^{(\mathrm{int})}(\xi,\zeta) = O_l(\xi,\zeta) + D_l(\xi,\zeta), \tag{30}$$

where

$$O_l(\xi,\zeta) = \int_{|n_{//}|<\frac{1}{n_1}} T(n_{//}) \frac{e^{in_1\chi\sqrt{1-n_{//}^2}}}{\sqrt{1-n_{//}^2}} e^{il\arccos(n_{//})} e^{-i\sqrt{1-n_1^2n_{//}^2}(\xi+\chi)} e^{in_1n_{//}\zeta} dn_{//} \tag{31}$$

and

$$D_l(\xi,\zeta) = \int_{\frac{1}{n_1}<|n_{//}|<1} T(n_{//}) \frac{e^{in_1\chi\sqrt{1-n_{//}^2}}}{\sqrt{1-n_{//}^2}} e^{il\arccos(n_{//})} e^{\sqrt{n_1^2n_{//}^2-1}(\xi+\chi)} e^{in_1n_{//}\zeta} dn_{//}. \tag{32}$$

Note that the present decomposition is linked to a physical phenomenon: in fact all the components of the homogeneous spectrum are totally reflected when $|n_{//}| > 1/n_1$.

- **Integration of $O_l(\xi, \zeta)$**

In order to point out the oscillating behavior of the integrand in Eq. (31), let us make the position $n_{//} = \cos(t)$, thus obtaining:

$$\begin{aligned} O_l(\xi,\zeta) &= \int_{t_1}^{t_2} T[\cos(t)] e^{i\left[-\sqrt{1-n_1^2\cos^2(t)}(\xi+\chi)+n_1\zeta\cos(t)+n_1\chi\sin(t)+lt\right]} dt \\ &= \int_{t_1}^{t_2} T[\cos(t)] e^{i\gamma(t)} dt, \end{aligned} \tag{33}$$

where $t_1 = \arccos(1/n_1)$, $t_2 = \arccos(-1/n_1)$, and

$$e^{i\gamma(t)} = e^{i\left[-\sqrt{1-n_1^2\cos^2(t)}(\xi+\chi)+n_1\zeta\cos(t)+n_1\chi\sin(t)+lt\right]}. \tag{34}$$

In practical cases, the term $T[\cos(t)]$ is a fairly regular function and does not greatly affect the integration technique. The kernel $e^{i\gamma(t)}$, instead, shows a highly oscillating behavior as the parameters ξ, ζ, χ, and l, increase; moreover, this kernel presents an oscillation rate which is a nonlinear function of the integration variable.

To integrate Eq. (33), we take as a starting point the adaptive generalized Gaussian quadrature rule proposed in [15], which is based on a decomposition of the integration interval in a suitable number of subdomains; the number of subdomains and their amplitudes depend on the oscillatory behavior of the integrand. The abovementioned adaptive integration algorithm, however, is based on the assumption that the local oscillation rate is monotonic; on the other hand, in the present case the oscillation rate

$$\begin{aligned} f_i(t) &= \frac{1}{2\pi}\left|\frac{d\gamma(t)}{dt}\right| \\ &= \frac{1}{2\pi}\left|\frac{-n_1\sin(2t)}{2\sqrt{1-n_1^2\cos^2(t)}}(\xi+\chi) - n_1\zeta\sin(t) + n_1\chi\cos(t) + l\right| \end{aligned} \tag{35}$$

is not a monotonic function, as one can see, when the parameters n_1, ξ, ζ, χ, and l vary. Therefore, in order to calculate the integral in Eq. (33), it is necessary to make a previous decomposition of the whole interval in a suitable number of subintervals in which $f_i(t)$ behaves monotonically.

By using the adaptive algorithm, we obtained the decomposition of the integration domain in subintervals shown in Fig. 3, as an example.

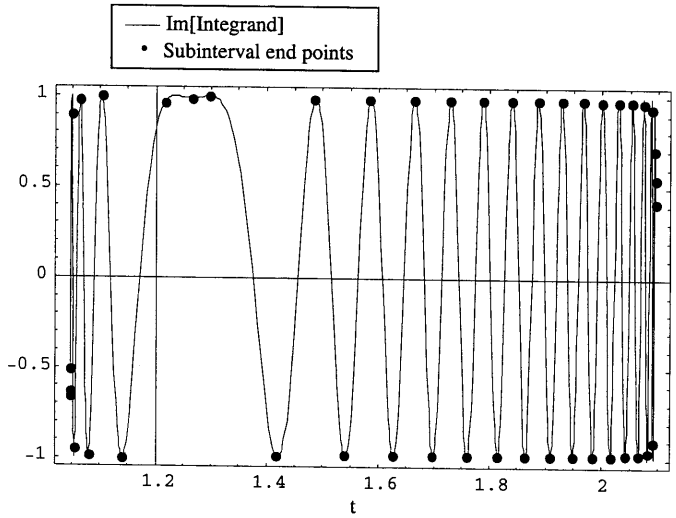

Figure 3. Imaginary part of the oscillating integrand of Eq. (33), shown together with its subinterval end points, when $T[\cos(t)] = 1$, $\xi = -50$, $\zeta = 10$, $\chi = 3$, $l = -50$, and $n_1 = 2$.

The imaginary part of the oscillating integrand of Eq. (33) is shown together with its subinterval end points, when $T[\cos(t)] = 1$, $\xi = -50$, $\zeta = 10$, $\chi = 3$, $l = -50$ and $n_1 = 2$. It can be noted that, even if the number of oscillations of the integrand is high, the adaptive algorithm is able to track them.

- **Integration of** $D_l(\xi, \zeta)$

The integral of Eq. (32) is the contribution of the totally reflected components of the homogeneous spectrum. In order to remove the singularity of the integrand function in $n_{//} = \pm 1$, we put $n_{//} = \cos(t)$ and rewrite Eq. (32) as follows:

$$D_l(\xi,\zeta) = \int_0^{t_1} T[\cos(t)] e^{i[n_1\zeta\cos(t)+n_1\chi\sin(t)+lt]} e^{\sqrt{n_1^2\cos^2(t)-1}(\xi+\chi)} dt + \int_{t_2}^{\pi} T[\cos(t)] e^{i[n_1\zeta\cos(t)+n_1\chi\sin(t)+lt]} e^{\sqrt{n_1^2\cos^2(t)-1}(\xi+\chi)} dt. \quad (36)$$

Making use of the parity property of the transmission coefficient ($T[\cos(\pi - t)] = T[\cos(t)]$), the second integral in Eq. (36) can be

expressed as a function of the first integral, obtaining:

$$D_l(\xi,\zeta) = D_l^{(1)}(\xi,\zeta) + (-1)^l D_{-l}^{(1)}(\xi,-\zeta), \tag{37}$$

where

$$D_l^{(1)}(\xi,\zeta) = \int_0^{t_1} T[\cos(t)] e^{i[n_1\zeta\cos(t)+n_1\chi\sin(t)+lt]} e^{\sqrt{n_1^2\cos^2(t)-1}(\xi+\chi)} dt. \tag{38}$$

Therefore, only the integration of $D_l^{(1)}(\xi,\zeta)$ has to be performed.

The integrand in Eq. (38) is the product of a purely oscillating function, showing an oscillation rate which is a nonlinear function of the integration variable, times an exponentially decreasing function (in fact, in medium 0 it is always $\xi + \chi < 0$). As the parameters ζ, χ and l increase, the oscillating rate increase too, causing an irregular behavior of the integrand function. As ξ increases, the exponential becomes predominant and the integrand function rapidly approaches 0, with negligible oscillations. Due to the just discussed peculiarities, the integration requirements are similar to the case of the homogeneous contribution $O_l(\xi,\zeta)$ and a similar adaptive generalized Gaussian quadrature rule has been developed.

In Fig. 4 the real part of the oscillating integrand of Eq. (38) is shown together with its subinterval end points chosen by the adaptive decomposition algorithm, when $T[\cos(t)] = 1$, $\xi = -4$, $\zeta = 190$, $\chi = 3$, $l = -10$ and $n_1 = 2$. It can be noted that the adaptive algorithm chooses the integrand extrema as subintervals endpoints.

4. NUMERICAL RESULTS

In the following, we use the mathematical tools presented in Sects. 2 and 3 to obtain numerical results for the diffracted-transmitted field V_{dt} (in medium 0), both in TM (Sect. 4.1) and TE (Sect. 4.2) polarizations. We show the effects of the variation of the normalized cylinder-interface distance χ, the refractive index n_1 of the medium in which the cylinder is buried, the incidence angle φ, and the normalized cylinder radius α. In all shown plots, medium 1 is an isotropic lossless dielectric.

4.1. TM Polarization

In TM polarization, V_{dt} corresponds to the electrical field E_{dt} diffracted by the cylinder and transmitted in medium 0 through the plane interface.

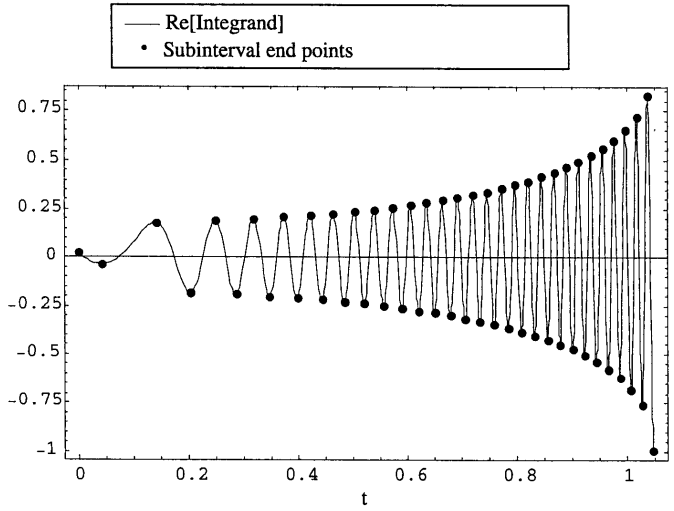

Figure 4. Real part of the oscillating integrand of Eq. (38), shown together with its subinterval end points, when $T[\cos(t)] = 1$, $\xi = -4$, $\zeta = 190$, $\chi = 3$, $l = -10$, and $n_1 = 2$.

In Fig. 5(a) a schematic drawing of the geometrical layout is sketched. In Fig. 5(b), the modulus of the diffracted-transmitted electrical field $|E_{\rm dt}|$ in proximity of the interface, is shown as a function of ζ; the incident plane wave impinges on the plane interface normally ($\varphi = 0$), $\alpha = 1$, $n_1 = 2$, $\xi = -\chi - 0.1$ where $\chi = \alpha + \pi/2$. It can be noted that there is a maximum of the field in the same direction from which the incident plane wave impinges; moreover, the plot is symmetrical with respect to $\zeta = 0$, as is correct in case of normal incidence. To check the convergence properties of our technique we show, in Fig. 6, the behavior of the modulus of the expansion coefficients C_l in Eq. (21) for different values of the truncation index ($M = 1$, 3, 9, 15) for the case of Fig. 5(b). It is noted that, apart from the case $M = 1$, all the other results are coincident, showing the validity of the criterion $M \cong 3\alpha$. A typical estimation of the computer time for our FORTRAN code is about 50 ms to obtain one point in Fig. 5(b) on a Pentium III, 500 MHz, with 64 MB RAM. To give a global idea of the behavior of the field as a function of the ξ coordinate, in Fig. 7 a plot of $|E_{\rm dt}|$, as a function of ξ and ζ, is reported for the same case of Fig. 5(b).

In Fig. 8, eleven contour plots of $|E_{\rm dt}|$, as a function of ξ and ζ, are reported, for $\varphi = 0$, $\alpha = 1$, and $n_1 = 2$. In the generic plot, we have $\chi = \alpha + \frac{2\pi}{10} j$, with the integer $j = 0, 1, ..., 10$. To increase

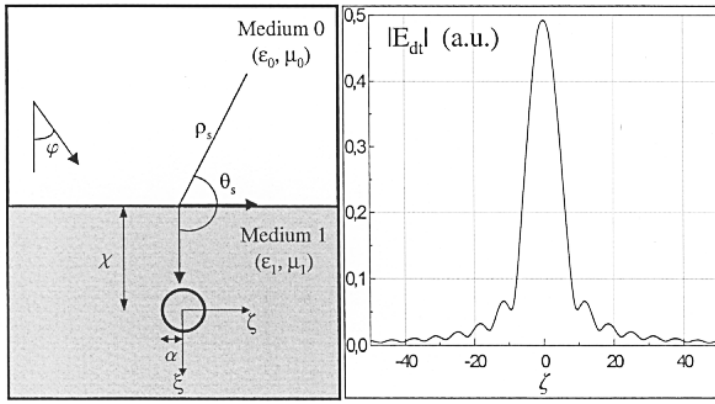

Figure 5. (a) Schematic drawing of the geometrical layout. (b) $|E_{\rm dt}|$, in arbitrary units, vs. ζ; TM polarization, $\varphi = 0$, $\alpha = 1$, $n_1 = 2$; the electrical field is evaluated in $\xi = -\chi - 0.1$ where $\chi = \alpha + \pi/2$.

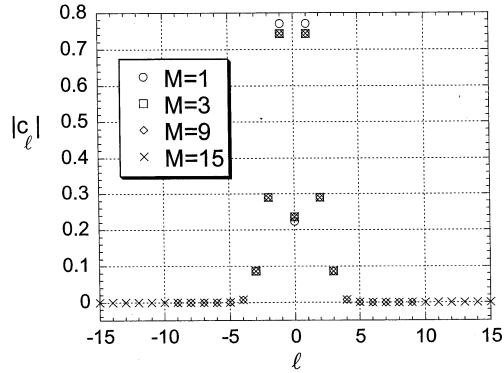

Figure 6. Modulus of the expansion coefficients C_l in Eq. (21) for different values of the truncation index ($M = 1$, 3, 9, 15) for the case of Fig. 5(b).

the visibility, each plot is normalized to its maximum $|E_{\rm dt}|_{\rm MAX}$ and ranges from black ($|E_{\rm dt}| = 0$) to white ($|E_{\rm dt}| = |E_{\rm dt}|_{\rm MAX}$); a change in the gray scale between two adjacent regions corresponds to a field variation of 10%. It can be noted that, as χ increases, the main lobe of $|E_{\rm dt}|$ becomes wider. Moreover, $|E_{\rm dt}|_{\rm MAX}$ decreases, as apparent from the lower-right diagram, where it is reported for the considered cases; the shown values highlight that, as χ increases, $|E_{\rm dt}|_{\rm MAX}$ does not

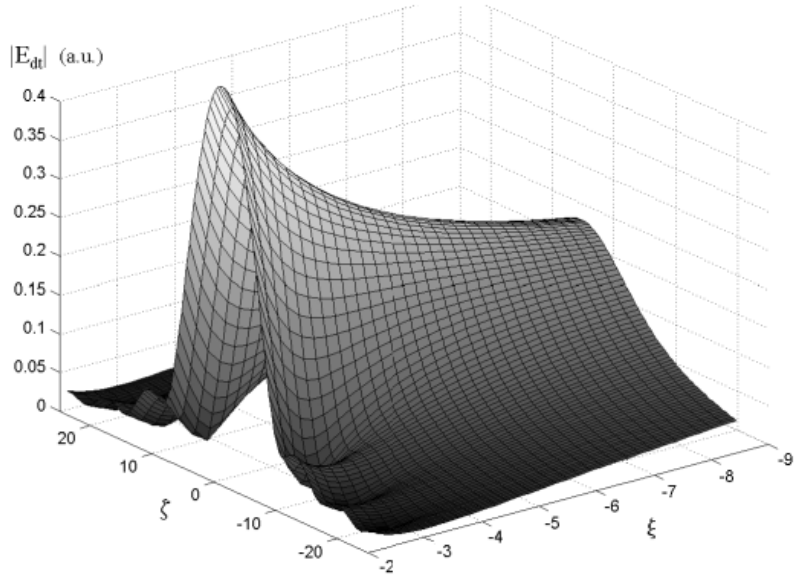

Figure 7. Plot of $|E_{\rm dt}|$ (near field), in arbitrary units, vs. ξ and ζ; $-\chi - 2\pi \leq \xi \leq -\chi$ and $-8\pi \leq \zeta \leq 8\pi$; the remaining parameters are the same of Fig. 5(b).

decrease monotonically: the oscillations are due to multiple reflections, which depend on the relative position between the cylinder and the plane interface. In Fig. 9 four field maps of the modulus of diffracted-transmitted electrical near field, as a function of ξ and ζ, are reported. The gray scale of each plot ranges from black ($|E_{\rm dt}| = 0$) to white ($|E_{\rm dt}| = |E_{\rm dt}|_{\rm MAX}$). The plots refer to different choices of the refractive index of medium 1: $n_1 = 1.3,\ 2,\ 4,\ 10$. The other parameters are: $\varphi = 0$, $\alpha = 1$, $\chi = 3$. The plots highlight that, as n_1 increases, $|E_{\rm dt}|$ becomes less intense and its main lobe becomes narrower: in fact, more components of the spectrum undergo total reflection. The effects of the variation of n_1 can also be seen from Fig. 10, where $|E_{\rm dt}|$ is shown as a function of ζ, for the same situation of Fig. 9, in $\xi = -\chi - 0.1$.

The effects of the variation of the incidence angle φ can be evaluated looking at Fig. 11; here, $|E_{\rm dt}|$ in the far region is shown, as a function of the scattering angle θ_s (see Fig. 5(a)), for different values of φ: $\varphi = 0^{\rm o}$ (a), $-30^{\rm o}$ (b), $-60^{\rm o}$ (c), $-75^{\rm o}$ (d); moreover, $\alpha = 5$, $\chi = 12.5$, and $n_1 = 1.3$. In [11], Naqvi *et al.* presented the corrections on a previous work [9], in which the Kobayashi [10] method was applied to the plane-wave scattering by a conducting cylinder buried in a

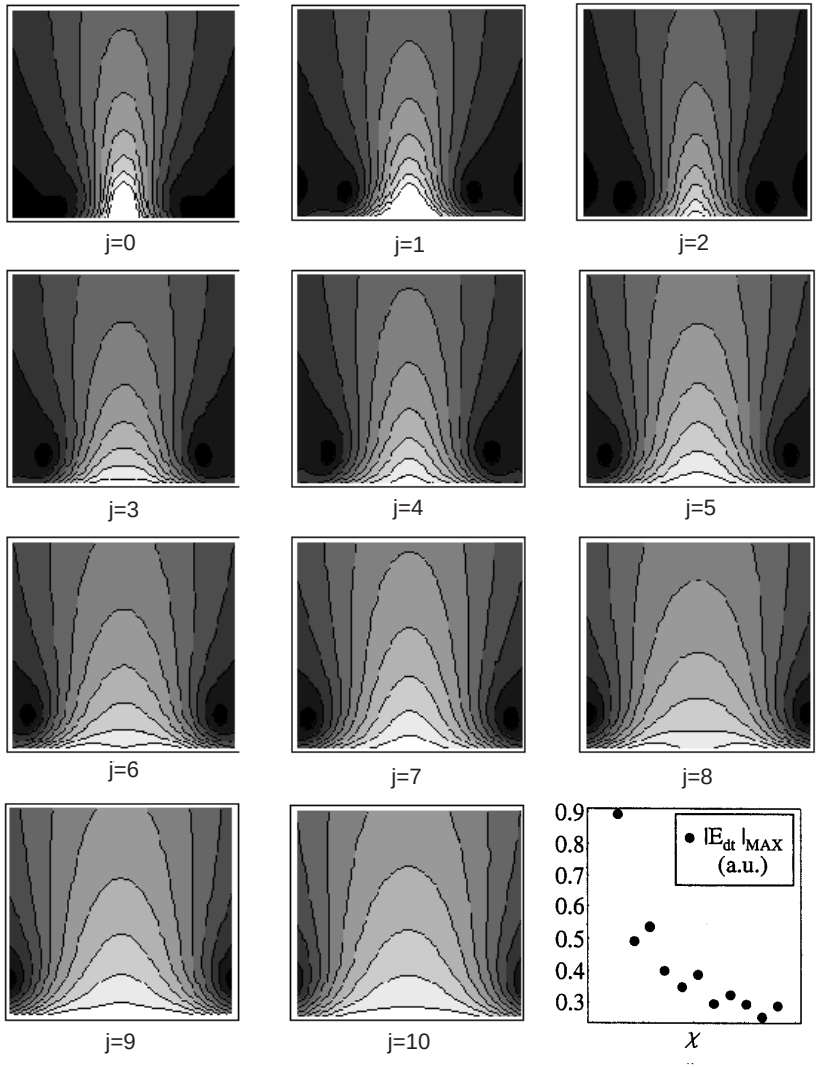

Figure 8. Contour plots of $|E_{\rm dt}|$, vs. ξ and ζ; TM polarization, $\varphi = 0$, $\alpha = 1$, $n_1 = 2$, $\chi = \alpha + \frac{2\pi}{10}j$, with the integer $j = 0, 1, ..., 10$; $-\chi - 2\pi \leq \xi \leq -\chi$ and $-4\pi \leq \zeta \leq 4\pi$. In the lower-right corner, $|E_{\rm dt}|_{\rm MAX}$ (a.u.) is shown for the considered cases.

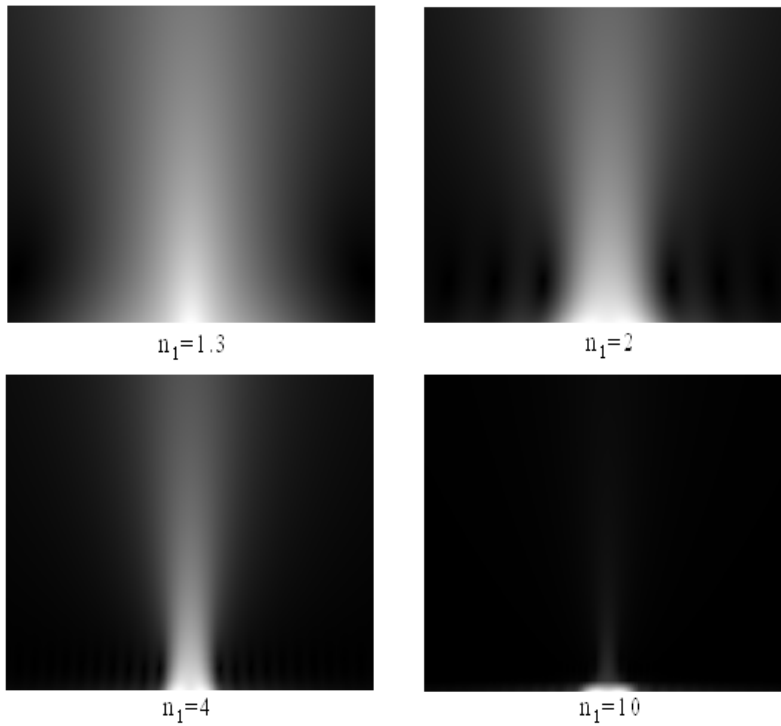

Figure 9. Bidimensional field maps of $|E_{\rm dt}|$, vs. ξ and ζ; TM polarization, $\varphi = 0$, $\alpha = 1$, $\chi = 3$, $-\chi - 2\pi \leq \xi \leq -\chi$ and $-8\pi \leq \zeta \leq 8\pi$.

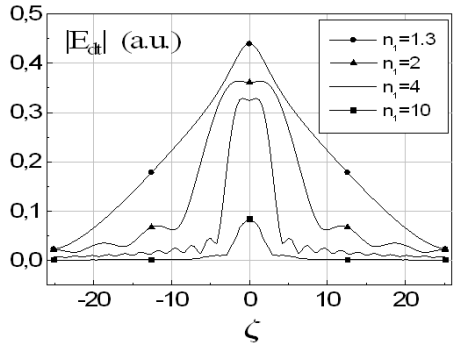

Figure 10. $|E_{\rm dt}|$ (a.u.) vs. ζ, for the same cases as in Fig. 9, in $\xi = -\chi - 0.1$.

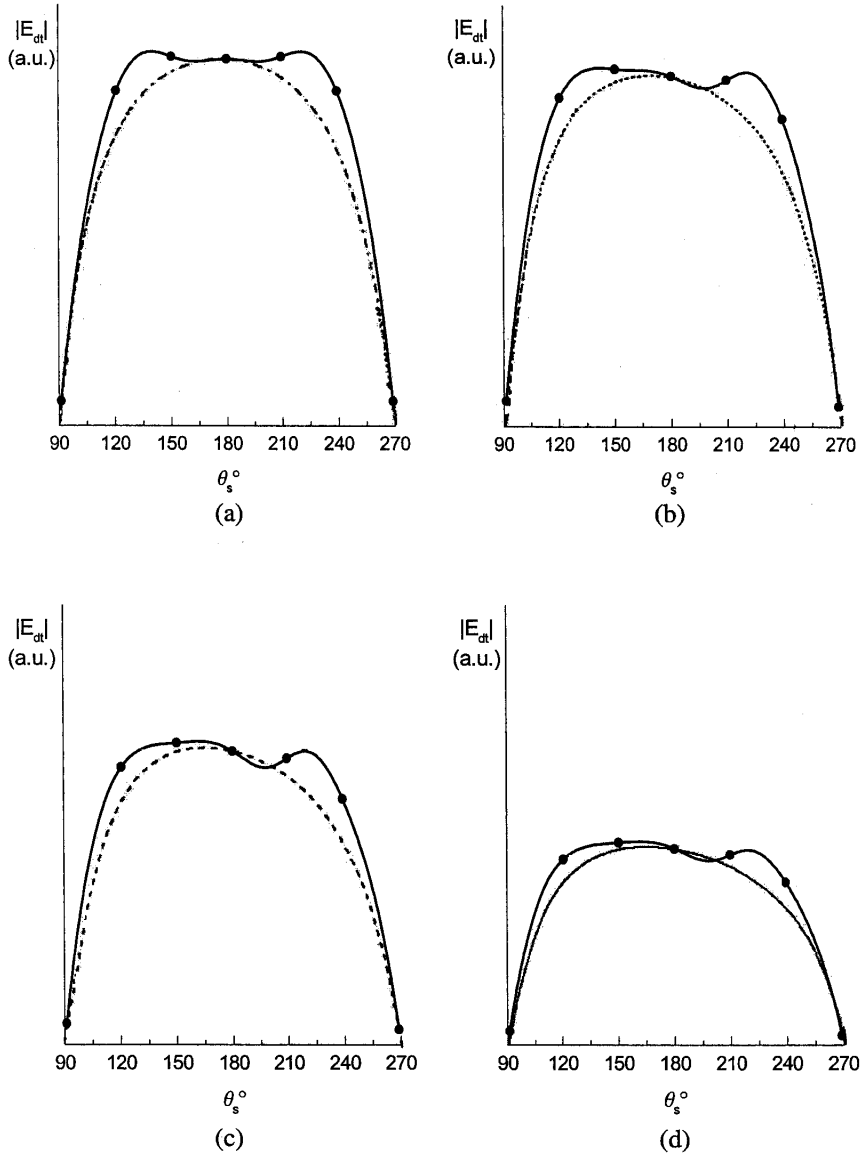

Figure 11. $|E_{\rm dt}|$, vs. the scattering angle θ_s, for $\varphi = 0^{\rm o}\ (a), -30^{\rm o}\ (b), -60^{\rm o}\ (c), -75^{\rm o}\ (d)$; TM polarization, $\alpha = 5$, $\chi = 12.5$, and $n_1 = 1.3$. Full line with dots: our results; the other lines: results in [11].

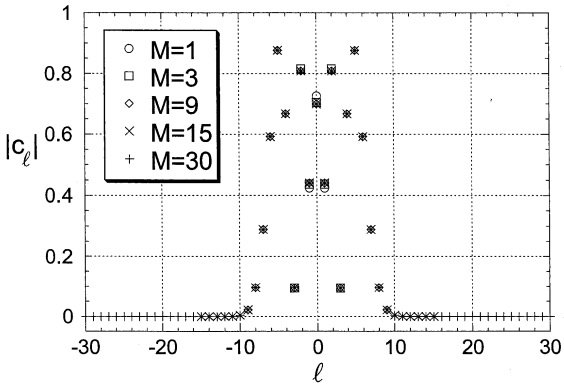

Figure 12. Modulus of the expansion coefficients C_l in Eq. (21) for different values of the truncation index ($M = 1$, 3, 9, 15, 30) for the case of Fig. 11.

dielectric medium. The plots reported in Fig. 11 are directly compared with Fig. 5 of [11], for which the same parameters have been used. We plotted our results in arbitrary units, normalized with respect to the maximum of Naqvi's curve for normal incidence. The largest difference between our results and Naqvi's is of about 15%. Our results show the presence of a greater dependence on the scattering angle in the field pattern, than in [11]: actually, due to the quite big size of the cylinder, one can expect such a behavior be present in the scattered far field [22, 23]. Finally, it is noted that the position of the minimum in our curves is roughly independent of the incidence angle: such result is in agreement with a previous paper [13] in the case, here considered, of TM polarization.

In Fig. 12 we show again the modulus of the expansion coefficients C_l in Eq. (21) for different values of the truncation index ($M = 1$, 3, 9, 15, 30) for the case of Fig. 11. The results for $M = 9$ are still coincident up to the fourth significant figure. Therefore also in this case the rule of thumb $M \cong 3\alpha$ is well satisfied.

In Fig. 13, $|E_{\rm dt}|$ in the near-field region is shown, as a function of ζ, for the same parameters of Fig. 11, and $\xi = -13.5$. From Figs. 11 and 13 the effects of a variation of the incidence angle are apparent, i.e., moving from normal incidence, $|E_{\rm dt}|_{\rm MAX}$ decreases and the main lobe changes slightly its shape.

In Fig. 14, $|E_{\rm dt}|$ is plotted as a function of ζ, when $\varphi = 0$, and $n_1 = 2$. Different values of the cylinder radius are considered: $\alpha = 0.1, 1, 5, 10$; moreover $\chi = \alpha + \pi/2$. In Fig. 14(a) $|E_{\rm dt}|$ in the near region is shown when $\xi = -\chi - 0.1$, while in Fig. 14(b) the far field is

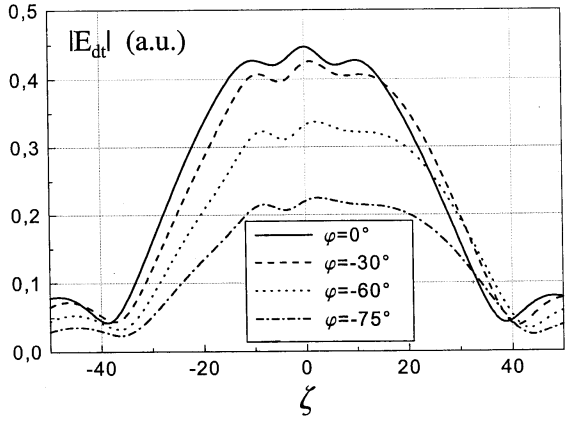

Figure 13. $|E_{\rm dt}|$, vs. ζ, for the same parameters of Fig. 11, when $\xi = -13.5$.

plotted. It can be noted that the increase of the cylinder radius causes a growth of $|E_{\rm dt}|$ and the presence of more pronounced secondary lobes: a similar behavior occurs in the case of scattering by a cylinder in free-space [22, 23].

4.2. TE Polarization

In TE polarization, $V_{\rm dt}$ corresponds to the magnetic field diffracted by the cylinder and transmitted in medium 0 through the plane interface. By using the partial derivatives of $V(\xi, \zeta)$, $|E_{\rm dt}|$ can be obtained and it is possible to make a comparison with the results of TM polarization.

In Fig. 15, $|E_{\rm dt}|$ is plotted when $\varphi = 0$, $n_1 = 2$, $\alpha = 1$, and $\chi = \alpha + \pi/2$. In Fig. 15(a), results are reported, as a function of ξ and ζ, for TM polarization, while in Fig. 15(b) the polarization is TE. For a better clearness, relevant gray-scale plots are shown in Figs. 15(c) and 15(d), respectively. It is seen that in TM polarization the main lobe is slightly tighter and $|E_{\rm dt}|$ shows a higher maximum. Moreover, in TE polarization there are more prominent lateral oscillations. Therefore, it is apparent that, in the near region, while in TM polarization $E_{\rm dt}$ is mainly focused in the incidence direction, in TE polarization the field is more diffused. In Fig. 15(e), finally, a plot of $|E_{\rm dt}|$ in the far-field zone is presented, as a function of θ_s, for both TM and TE polarizations. The order of magnitude is the same for both polarizations. The patterns show a mild dependence on the scattering angle: these results are again similar to those reported in [22] for the case of an isolated cylinder.

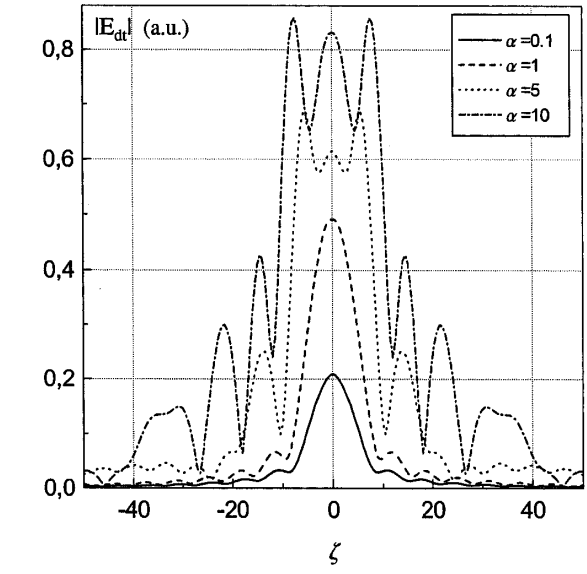

(a)

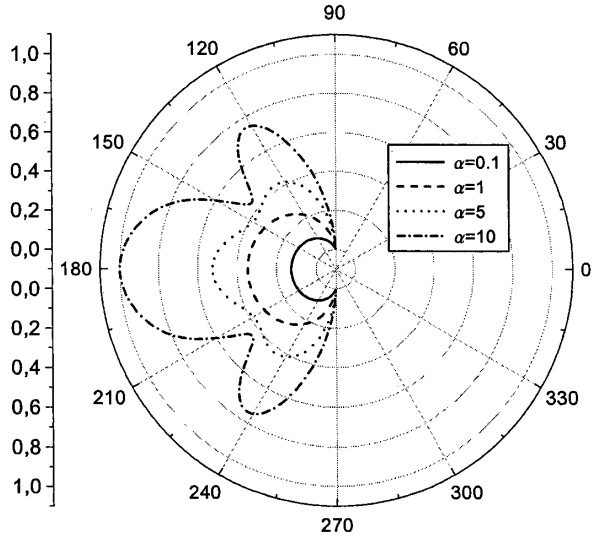

(b)

Figure 14. (a) $|E_{\rm dt}|$, vs. ζ, when $\varphi = 0$, $n_1 = 2$, TM polarization, and $\alpha = 0.1, 1, 5, 10$; $\chi = \alpha + \pi/2$, $\xi = -\chi - 0.1$. (b) Far-field plot, for the same parameters as in (a).

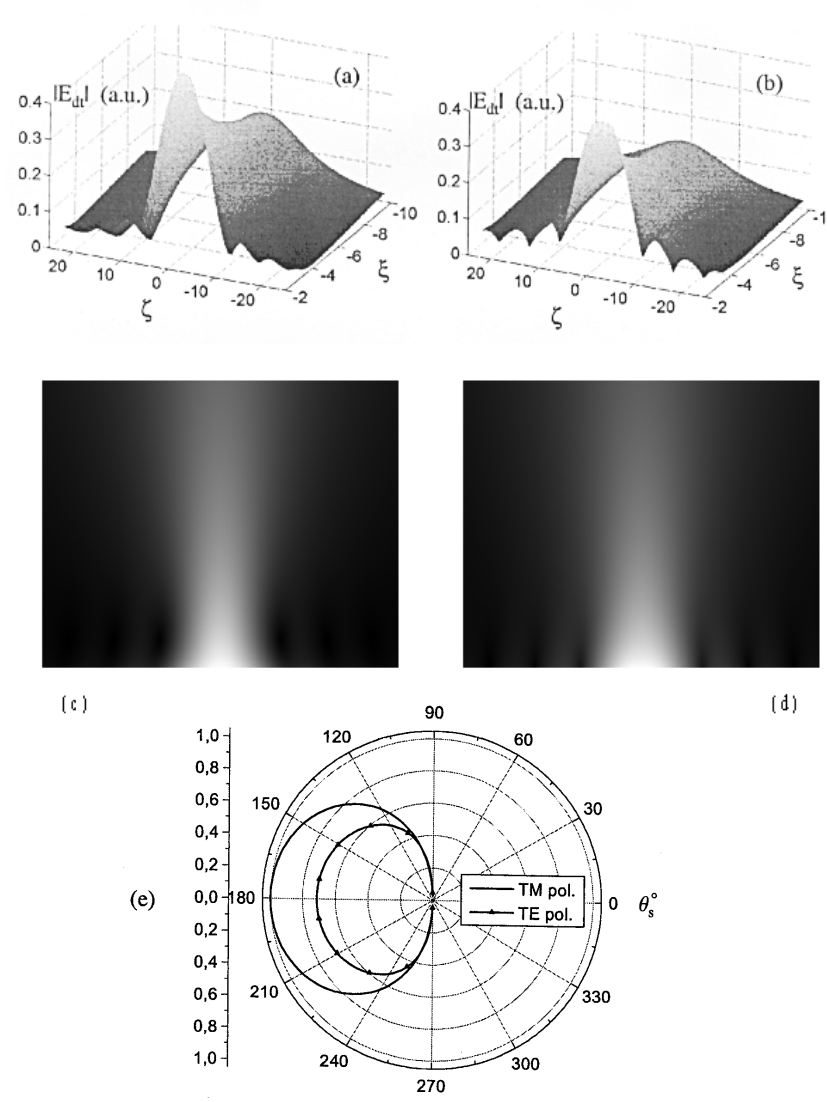

Figure 15. Plots of $|E_{\rm dt}|$ (a.u.), when $\varphi = 0$, $n_1 = 2$, $\alpha = 1$, and $\chi = \alpha + \pi/2$. (a) and (c): $|E_{\rm dt}|$, vs. ξ and ζ ($-\chi - 2\pi \leq \xi \leq -\chi$ and $-8\pi \leq \zeta \leq 8\pi$), TM polarization; (b) and (d): same as (a) and (c), TE polarization; (e) $|E_{\rm dt}|$, in far-field zone, as a function of θ_s, for both TM and TE polarization.

5. CONCLUSION

A spectral-domain solution has been employed to completely characterize the two-dimensional plane-wave scattering problem of a perfectly conducting circular cylinder buried in a dielectric half-space. It is noted that the general frame of our theory could also be used to deal with complex values of the wavenumber in medium 1, to take into account the presence of losses; however, in this case the spectral integrals must be suitably performed in the complex plane.

Both TM and TE polarization cases have been treated and results are presented for both near and far fields, showing the influence of the various parameters involved. A comparison has been reported with recent results in the literature, showing a good agreement. The presented case is also of interest for more general incident fields as, for instance, pulse excitations [24]. Since it is customary to represent 2D scatterers of arbitrary shape by means of an array of cylinders [25], [26], our theory can be of interest also in that case. Finally, our procedure may be generalized to the dielectric-cylinder case, as is shown in [27].

APPENDIX A. DERIVATIVES OF THE CYLINDRICAL TRANSMITTED WAVE FUNCTIONS $TW_l(\xi,\zeta)$

We start from the definition of the function $TW_l(\xi,\zeta)$ (Eq. (13)):

$$TW_l(\xi,\zeta) = \frac{1}{2\pi}\int_{-\infty}^{+\infty} T(n_{//}^1)F_l(-n_1\chi, n_{//}^1)e^{-in_\perp^0(\xi+\chi)}e^{in_{//}^0\zeta}dn_{//}^1 \quad \text{(A1)}$$

and we obtain

$$\begin{aligned}\frac{\partial TW_l(\xi,\zeta)}{\partial\zeta} &= \frac{1}{2\pi}\int_{-\infty}^{+\infty} T(n_{//}^1)F_l(-n_1\chi, n_{//}^1)e^{-in_\perp^0(\xi+\chi)}\frac{\partial e^{in_{//}^0\zeta}}{\partial\zeta}dn_{//}^1 \\ &= \frac{in_1}{2\pi}\int_{-\infty}^{+\infty} n_{//}^1 T(n_{//}^1)F_l(-n_1\chi, n_{//}^1)e^{-in_\perp^0(\xi+\chi)}e^{in_1 n_{//}^1\zeta}dn_{//}^1\end{aligned} \quad \text{(A2)}$$

and

$$\frac{\partial TW_l(\xi,\zeta)}{\partial\xi} = \frac{1}{2\pi}\int_{-\infty}^{+\infty} T(n_{//}^1)F_l(-n_1\chi, n_{//}^1)\frac{\partial e^{-in_\perp^0(\xi+\chi)}}{\partial\xi}e^{in_{//}^0\zeta}dn_{//}^1$$

$$= -\frac{i}{2\pi}\int_{-\infty}^{+\infty} n_\perp^0 T(n_{//}^1) F_l(-n_1\chi, n_{//}^1) e^{-in_\perp^0(\xi+\chi)} e^{in_{//}^0\zeta} dn_{//}^1. \tag{A3}$$

Eq. (A2) can be written in a more compact way. To this aim, we consider the expression of $TW_{l+1}(\xi,\zeta)$:

$$\begin{aligned} TW_{l+1}(\xi,\zeta) &= \frac{1}{2\pi}\int_{-\infty}^{+\infty} T(n_{//}^1) F_{l+1}(-n_1\chi, n_{//}^1) e^{-in_\perp^0(\xi+\chi)} e^{in_{//}^0\zeta} dn_{//}^1 \\ &= \frac{1}{2\pi}\int_{-\infty}^{+\infty} T(n_{//}^1)\frac{2}{n_\perp^1} e^{i\left(|n_1\chi|n_\perp^1+(l+1)\arccos(n_{//}^1)\right)} e^{in_{//}^1\zeta} dn_{//}^1 \\ &= \frac{1}{2\pi}\int_{-\infty}^{+\infty} T(n_{//}^1) F_l(-n_1\chi, n_{//}^1) e^{i\arccos(n_{//}^1)} e^{-in_\perp^0(\xi+\chi)} \\ &\quad e^{in_{//}^0\zeta} dn_{//}^1. \end{aligned} \tag{A4}$$

We take into account the trigonometric relation

$$e^{i\arccos(n_{//}^1)} = \cos[\arccos(n_{//}^1)] + i\sin[\arccos(n_{//}^1)] = n_{//}^1 + in_\perp^1, \tag{A5}$$

and Eq. (A4) becomes

$$\begin{aligned} TW_{l+1}(\xi,\zeta) = &\frac{1}{2\pi}\int_{-\infty}^{+\infty} n_{//}^1 T(n_{//}^1) F_{l+1}(-n_1\chi, n_{//}^1) e^{-in_\perp^0(\xi+\chi)} e^{in_{//}^0\zeta} dn_{//}^1 \\ &+\frac{i}{2\pi}\int_{-\infty}^{+\infty} n_\perp^1 T(n_{//}^1) F_l(-n_1\chi, n_{//}^1) e^{-in_\perp^0(\xi+\chi)} e^{in_{//}^0\zeta} dn_{//}^1. \end{aligned} \tag{A6}$$

By using Eq. (A2), and calling A_l the second integral in Eq. (A6), we get the following expression for $TW_{l+1}(\xi,\zeta)$:

$$TW_{l+1}(\xi,\zeta) = \frac{1}{in_1}\frac{\partial TW_l(\xi,\zeta)}{\partial\zeta} + A_l. \tag{A7}$$

Proceeding in the same way for $TW_{l-1}(\xi,\zeta)$, we find:

$$TW_{l-1}(\xi,\zeta) = \frac{1}{in_1}\frac{\partial TW_l(\xi,\zeta)}{\partial\zeta} - A_l. \tag{A8}$$

Adding Eqs. (A7) and (A8), we finally obtain:

$$\frac{\partial TW_l(\xi,\zeta)}{\partial \zeta} = \frac{in_1}{2}[TW_{l+1}(\xi,\zeta) + TW_{l-1}(\xi,\zeta)]. \tag{A9}$$

Note that, unlike in the case of the cylindrical reflected wave functions [13], it is possible to express a recurrence property only for the partial derivative of $TW_l(\xi,\zeta)$ with respect to ζ: this is due to the fact that, going through the interface from medium 1 to medium 0, the parallel component of the wavevector preserves itself, while the orthogonal component changes (see Eq.(12)).

REFERENCES

1. Howard, A. Q., "The electromagnetic fields of a subterranean cylindrical inhomogeneity excited by a line source," *Geophys.*, Vol. 37, 975–984, Dec. 1972.
2. Lambert, M., "The scattering by a cylindrical dielectric obstacle buried in a half-space: a H-field-based solution method," *J. of Electromagnetic Waves and Appl.,* Vol. 9, 1129–1262, Sept. 1998.
3. Parry, J. R. and S. H. Ward, "Electromagnetic scattering from cylinders of arbitrary cross-section in a conductive half-space," *Geophys.*, Vol. 36, 67–100, Feb. 1971.
4. Moaveni, M. K., A. A. Rizvi, and B. A. Kamran, "Plane-wave scattering by gratings of conducting cylinders in an inhomogeneous and lossy dielectric," *J. Opt. Soc. Am. A*, Vol. 5, 834–842, 1988.
5. Ogunade, S. O., "Electromagnetic response of an embedded cylinder for line current excitation," *Geophys.*, Vol. 46, 45–52, Jan. 1981.
6. D'Yakonov, B. P., "The diffraction of electromagnetic waves by a circular cylinder in a homogeneous half-space," *Bull. Acad. Sci. U.S.S.R., Geophysics,* ser. No. 9, 950–955, 1959.
7. Mahmoud, S. F., S. M. Ali, and J. R. Wait, "Electromagnetic scattering from a buried cylindrical inhomogeneity inside a lossy earth," *Radio Sci.*, Vol. 16, No. 6, 1285–1298, 1981.
8. Butler, C. M., X. B. Xu, and A. W. Glisson, "Current induced on a conducting cylinder located near the planar interface between two semi-infinite half-spaces," *IEEE Trans. Antennas Propagat.*, Vol. AP–33, 616–624, June 1985.
9. Hongo, K. and A. Hamamura, "Asymptotic solutions for the scattered field of plane wave by a cylindrical obstacle buried in a

dielectric half-space," *IEEE Trans. Antennas Propagat.*, Vol. AP–34, 1306–1312, Nov. 1986.

10. Sneddon, I. N., *Mixed Boundary Value Problems in Potential Theory*, North-Holland, Amsterdam, 1966.
11. Naqvi, Q. A., A. A. Rizvi, and Z. Yaqoob, Corrections to: "Asymptotic solutions for the scattered fields of plane wave by a cylindrical obstacle buried in a dielectric half-space," *IEEE Trans. Antennas Propagat.*, Vol. AP-48, 846–848, May 2000.
12. Cincotti, G., F. Gori, M. Santarsiero, F. Frezza, F. Furnò, and G. Schettini, "Plane wave expansion of cylindrical functions," *Opt. Commun.*, Vol. 95, 192–198, Jan. 1993.
13. Borghi, R., F. Frezza, F. Gori, M. Santarsiero, and G. Schettini, "Plane wave scattering by a perfectly conducting cylinder near a plane surface: cylindrical wave approach," *J. Opt. Soc. Am. A*, Vol. 13, 483–493, March 1996.
14. Borghi, R., F. Frezza, C. Santini, M. Santarsiero, and G. Schettini, "Numerical study of the reflection of cylindrical waves of arbitrary order by a generic planar interface," *J. of Electromagnetic Waves and Appl.*, Vol. 13, 27–50, Jan. 1999.
15. Borghi, R., F. Frezza, C. Santini, M. Santarsiero, and G. Schettini, "A quadrature algorithm for the evaluation of a 2D radiation integral with highly oscillating kernel," *J. of Electromagnetic Waves and Appl.*, Vol. 14, 1353–1370, Oct. 2000.
16. Daniels, D. J., *Surface-Penetrating Radar*, IEE, London, 1996.
17. Gurel, L. and U. Oguz, "Three-dimensional FDTD modeling of a ground-penetrating radar," *IEEE Trans. Geosci. and Remote Sensing*, Vol. 38, 1513–1521, July 2000.
18. Abramowitz, M. and A. Stegun, *Handbook of Mathematical Functions*, Dover Pub. Inc., New York, 1972.
19. Ragheb, H. A. and M. Hamid, "Scattering by N parallel conducting circular cylinders," *Int. J. Electron.*, Vol. 59, 407–421, 1985.
20. Elsherbeni, A. Z., "A comparative study of two-dimensional multiple scattering techniques," *Radio Sci.*, Vol. 29, 1023–1033, 1994.
21. Blakemore, M., G. A. Evans, and J. Hysop, "Comparison of some methods for evaluating infinite range oscillatory integrals," *J. Comput. Phys.*, Vol. 22, 352–376, 1976.
22. Bowman, J. J., T. B. Senior, and P. L. E. Uslenghi, *Electromagnetic and Acoustic Scattering by Simple Shapes*, Hemisphere, New York, 1970.

23. Balanis, C. A., *Advanced Engineering Electromagnetics*, Ch. 11, John Wiley & Sons, New York, 1989.
24. Vitebskiy, S., K. Sturgess, and L. Carin, "Short-pulse plane-wave scattering from buried perfectly conducting bodies of revolution," *IEEE Trans. Antennas Propagat.,* Vol. AP-44, 143–151, Feb. 1996.
25. Ragheb, H. A. and M. Hamid, "Simulation of a cylindrical reflector by conducting circular cylinders," *IEEE Trans. Antennas Propagat.,* Vol. AP-35, 349–353, Mar. 1987.
26. Elsherbeni, A. Z. and A. A. Kishk, "Modeling of cylindrical objects by circular dielectric and conducting cylinders," *IEEE Trans. Antennas Propagat.,* Vol. AP-40, 96–99, Jan. 1992.
27. Borghi, R., M. Santarsiero, F. Frezza, and G. Schettini, "Plane-wave scattering by a dielectric circular cylinder parallel to a general reflecting flat surface," *J. Opt. Soc. Am. A,* Vol. 14, 1500–1504, 1997.